Non-Premixed Lifted Flame Stabilization Coupled with Vortex Structures in a Coaxial Jet

Aurélie Wyzgolik, Françoise Baillot

CORIA-UMR 6614, CNRS-Université et INSA de Rouen, CORIA, BP 12, 76801 SAINT ETIENNE DU ROUVRAY CEDEX , France

1 Introduction

This paper concerns the study of the non-premixed lifted flame stabilization mechanisms. The understanding of these mechanisms is always a challenge for technological engine and furnace design: in addition to safety, it is necessary that the future combustion chambers improve their effectiveness in order to reduce costs, to increase energy efficiency, and to diminish their emissions of pollutants and their noise levels. Several models, registered by Schefer et al. [1], have been proposed. Most of them have shown that the interaction between the flame and jet structures constitutes an important parameter for the flame behavior [2, 3, 4]. This feature has been underlined by Demare and Baillot [5] through their study about flames stabilized in *free organized* methane jets. There, two types of vortices developed: primary vortices due to the Kelvin-Helmholtz (KH) instability and streamwise vortices (filaments) due to secondary instabilities. Results showed that the flame did not stabilize on primary rings but on secondary vortices. The present work pursues this previous study by investigating the action of an air coflow on the central organized methane jet and, consequently, on the flame stabilization response. This configuration tends towards the industrial applications but also provides clear boundary conditions more easily implemented in numerical simulations when comparisons between experimental and numerical data are attempted. For that, the inner methane/air mixing layer is modified by imposing the gas flow rate velocity ratio (or equivalently the mixing ratio). In the literature, studies on turbulent configurations can be found that investigate the velocity field in the vicinity of the stabilization point [4, 6, 7]. The statistical treatment of the data showed that the flame stabilized in a region of relatively low velocity (mean axial velocity $\leq 3S_L$) but no attempt was made to analyze results on the basis of a fine identification of jet structures and their coupling with the flame base. Here, our study aims to focus on the vortex-flame interaction in order to explain changes in the flame behavior from a laminarized stabilization to a turbulent one. The jet dynamics, modified by adjusting the inner jet mixing layer, is determined by means of particle image velocimetry (PIV) and time resolved laser tomography. In particular we give attention to the evolution of primary and streamwise vortices.

2 Experimental set up

The non-premixed flame is fed by a methane jet with an outer air coflow. The burner consists of two vertical convergent tubes. The inner one has a 65mm diameter core and a 6mm diameter nozzle, Di, with a 0.2mm lip. The air coflow has a 266mm diameter core and a 66mm diameter nozzle, Do, with a lip thinner than 0.2mm. The flame base is not influenced by the quiet air as much as the base is prevented from it by the air coflow potential core, very long here (As=1-(Di/Do) ~ 1) [10]. The flow rate velocities are: $0<Uo<1$m/s for the air and Ui=10m/s for the methane. Hence, Reynolds number $Reo=Uo*(Do-Di)/(2\nu_{air})$ ranges from 0 to 2000 and $Rei=Ui*Di/\nu_{CH4}$ is 3600. With a lifted flame, it was experimentally verified that the vertical velocity profile at each nozzle exit is 'top-hat' and fluctuations are low (a few percent).
Two techniques are used to investigate the properties of the flows which can be separately seeded by olive oil droplets: first, high speed laser tomography using a digital camera Kodak Ektapro (8 bits, 9000 Hz) and an

Correspondence to : wyzgolik@coria.fr

Argon-ion continuous laser source (4 W, 515 nm). Second, PIV using a double-pulse laser. Time between a couple of pulses is chosen from 6 to 10 µs. Each beam has an energy of 40 mJ and is spread out into a sheet with a ~300mm thickness by a standard system of lenses. Only the cold part of the flow is accessible to measurement since the flame causes the evaporation of the oil droplets whose evaporation temperature is about 600K. Images are recorded by a CCD camera synchronized with the laser. To improve filament resolution, it was equipped with a macro objective which defines a field of ~13mm. PIV measurements are carried out in two types of sections: (i) vertical planes containing the jet axis. (ii) transverse planes, oriented at 21° in comparison with the horizontal plane, cutting the jet at various heights, in particular in the vicinity of the flame base. The image processing is ensured by the software V2IP© developed by CORIA laboratory based on a classical cross-correlation algorithm. It uses a 32*32 pixels² mesh with a 50% overlap for the transverse sections and a 64*64 pixels² mesh with a 75% overlap for the vertical cuts.

4 Automatic vortex identification

A criterion is introduced to identify vortices in order to automate the calculation of their characteristics from PIV fields. In the literature, various criteria are proposed; most of them are listed by Jeong and Hussain [8]. However, their formulations are based on the velocity gradient tensor, which is not easily calculable from PIV data. This problem is solved by introducing the vortex identification criterion proposed by Graftieaux et al. [9]. It needs to determine normalized kinetic moments $\vec{\sigma}_p(M)$ of points M located inside an area (S) of vector normal $\vec{n}$ and centred at point P. Hence, the topology of a velocity field is obtained by means of the normalized non-dimensional scalar function Γ_1(P) calculated by integrating $\vec{\sigma}_p(M).\vec{n}$ over (S). Γ_1, a Galilean invariant function, is positive when the identified structures have a counter-clockwise rotation. Here, (S) is chosen as a circle. Its radius R is a multiple of the PIV mesh side, Δ_{xy}. So, Γ_1(P) is approximated by the relationship:

$$\Gamma_1(P) = \frac{1}{N_1 \times {\Delta_{xy}}^2 + N_2 \times \left(\frac{\Delta_{xy}}{2}\right)^2} \left(\sum_{M \in S_1} \frac{\vec{PM}}{\left\| \vec{PM} \right\|} \wedge \frac{\vec{U}_M}{\left\| \vec{U}_M \right\|} . \vec{n} \quad {\Delta_{xy}}^2 + \sum_{M \in (S_2 \cap S)} \frac{\vec{PM}}{\left\| \vec{PM} \right\|} \wedge \frac{\vec{U}_M}{\left\| \vec{U}_M \right\|} . \vec{n} \quad \left(\frac{\Delta_{xy}}{2}\right)^2 \right)$$

with N_1(N_2): number of points of the PIV meshing in area (S_1) ((S_2)) ; (S_1): circle area with $R - \Delta_{xy}\sqrt{2}/2$ radius which only includes the meshes entirely inside (S); (S_2): annular area, with $R - \Delta_{xy}\sqrt{2}/2$ inner and $R + \Delta_{xy}\sqrt{2}/2$ outer radii, including the no-entire meshes of (S). The vortex centre is positioned at the local maximum of $|\Gamma_1|$. Then, other geometric and dynamic eddy characteristics can be calculated automatically.

5 Flame response and flow characteristics

A previous study of ours [10] in agreement with works on flames in a vitiated coflow [11] showed that depending on the coflow velocity, changes occurred in the flame behavior. For Ui=10m/s, the flame stabilized in its hysteresis zone for 0≤Uo≤0.49m/s and in its lift-off zone for Uo>0.49m/s. Moreover its physical features had been classified in two zones (Fig. 1), which was shown to be connected to the organization of the jet structures (KH vortices and filaments), introduced here in figure 2 (a and b). Zone A: for Uo≤0.37m/s, the flame is laminarized with a lobe-shaped base and a long yellow plume; its lift-off height slowly increases. The flame stabilizes on the filaments in the organized region, delimited by the end of the methane jet potential core. Horizontal tomography images recorded at the flame base with the air coflow only seeded, show the impact of the flame base as a horseshoe shape (Fig. 2c). Zone B: for Uo>0.37m/s, the flame loses its lobes and becomes turbulent with a tubular base; its height grows abruptly when the flame enters into zone B and keeps a stronger evolution than that one measured in zone A. It stabilizes in the turbulent zone. The circular shape of the flame impact, observed in horizontal tomography images, indicates that its wrinkled base is now composed of tips (Fig. 2d). So, the stabilization mechanism of the flame adapts to new conditions imposed by the air coflow adding. To refine the interpretation of these changes due to mixing layer modifications, quantify geometric and

dynamic characteristics of the jet structures is needed. In [10], a global approach pointed out that 'macro parameters' such as the two potential cores and inner jet spreading were efficient to describe the overall lifted flame behavior. In particular, the spreading, evaluated from the envelope of jet structures, got thinner with Uo increase. These results are now completed by a local approach in which physical quantities describing vortices are studied as functions of Uo. First, geometric parameters are determined: from horizontal tomography images, the filament length is measured at different distances from the burner exit, z in order to follow their development from their formation to the flame base locations. Moreover, instantaneous velocity fields provide radii of eddies in vertical cross-sections for primary structures (Fig. 3 and 4) and in transverse cross-sections for secondary ones (Fig. 5 and 6) from which a statistical analysis with Uo is carried out. The spreading jet is also quantified in vertical velocity fields by measuring angles, θ defined as angles between the direction of velocity vectors of an ejected filament and the horizontal plane. For that, vectors which deviate all together from the jet axis (D_F in Fig. 3) and which are included in the inner jet envelope (E in Fig. 3) are selected. θ is averaged from 500 vertical PIV fields and evaluated as a function of the radial distance, r from the jet axis. It appears that filaments vertically straighten as Uo increases. Second, dynamic characteristics are considered. The convection velocity of KH vortices is calculated from vertical tomography images (Fig. 2a) and compared with the classical theoretical formulation [12]. Furthermore, the rotating velocity U_θ of the KH vortices is obtained in vertical cross-sections (Fig. 3). For each vortex, an instantaneous profile of U_θ is calculated along specific lines (vertical or horizontal) whose origins are the vortex center (Fig. 4). The rotating velocity U_θ and the ejection velocity U_r of secondary structures are determined in transverse planes (Fig. 5). For a couple of streamwise vortices, two U_θ-profiles are measured along the line joining the two vortex cores and a U_r-profile along the streamline which intercepts the center of the segment delimited by the two previous cores (Fig. 6). These profiles give access to statistical data from which the behavior of vortices is determined as a function of Uo. So, the behavior of the flame is qualified with Uo.

6 Conclusion

This paper proposes to explain changes in the lifted flame from a laminar to a turbulent behavior induced by an air coflow by analyzing modifications of the air/methane mixing layer. To complete previous results based on a global approach [10], a systematic identification of vortices has been developed from a new criterion proposed by Graftieaux et al. [9]. Once located, vortices are quantified by means of local geometric and dynamic parameters giving a data base to obtain the evolution of eddies with Uo. This leads to a better understanding of the interaction between the flame stabilization and jet structures.

References

[1] Schefer R. W., Namazian M. and Kelly J. (1994). Comb. Fl. 99: 75–86.

[2] Chen M., Herrmann M. and Peters N. (2000). Proc. Comb. Inst. 28: 167-174.

[3] Favier V. and Vervisch L. (2001). Comb. Fl. 125: 788-803.

[4] Su L.K., Sun O.S. and Mungal M.G. Comb. and Fl. 144:494-512.

[5] Demare D. and Baillot F. (2001). Phys. Fluids. 13: 2662-2670.

[6] Muniz L. and Mungal M.G. (1997). Comb. Fl. 111:16-31.

[7] Watson K. A., Lyons K.M., Donbar J.M. and Carter C.D. (1999). Comb. and Fl. 117: 257-271.

[8] Jeong J. and Hussain F. (1995). J. Fluid Mech. 285: 69-94.

[9] Graftieaux L., Michard M. and Grosjean N. (2001). Meas. Sci. Technol. 12: 1422-1429.

[10] Wyzgolik A. Baillot F. (2007). Proc. of Comb. Inst. 31: 1583-1590.

[11] Cabra R., Chen J.-Y., Dibble R.W., Karpetis A.N., and Barlow R.S. (2005). Comb. Fl. 143:491-506.

[12] Bernal L.P. and Roshko A. (1986). J. Fluid Mech. 170: 499-525.

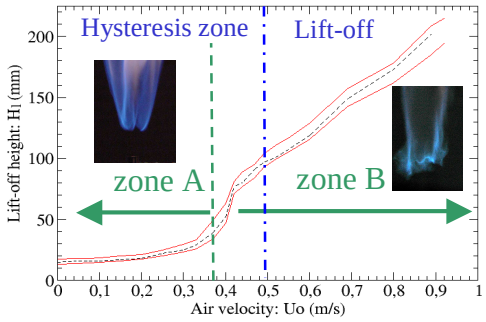

Fig.1: -- more probable lift-off height H_l, — $(H_l)_{rms}$. Zone A: lobe-shaped flame base domain; zone B: tubular flame base domain.

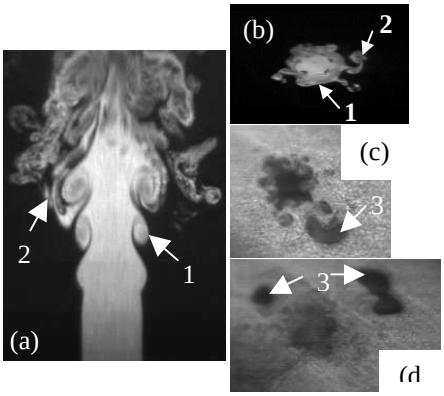

Fig.2: Laser tomography images: (a) vertical plane; (b, c, d) horizontal plane at the flame base. (a, b): methane seeding. (c, d): air seeding. (a, b, c): Uo=0.1m/s. (d) Uo=0.4m/s. (1) KH vortex, (2) filament, 3: flame impact (oil evaporation).

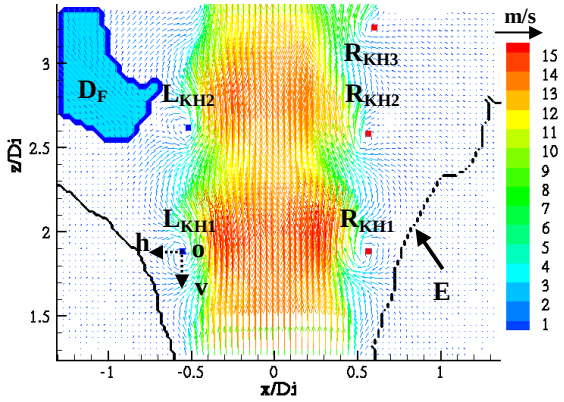

Fig.3: Vertical instantaneous velocity field at the flame base for Uo=0.1m/s. L_{KH1}-L_{KH2} (R_{KH1}-R_{KH3}): left (right) cut of KH rings, ov (oh): vertical (horizontal) line along which a U_θ-profile is measured, D_F: filament domain, E: inner jet envelope.

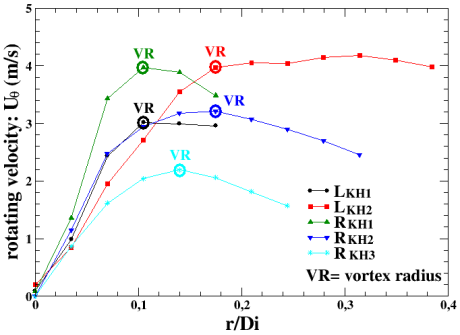

Fig.4: Instantaneous profiles of rotating velocity U_θ along vertical lines for KH vortices detected in the vertical PIV field shown in figure 3.

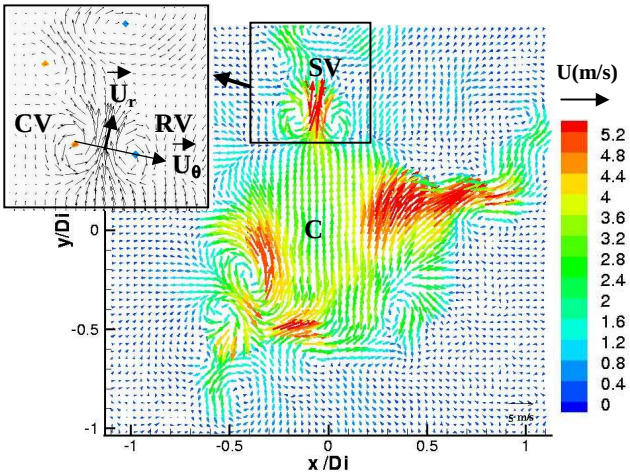

Fig.5: Instantaneous velocity field in a transverse plane at the flame base for Uo=0.1m/s. U: velocity norm, SV: streamwise vortices, C: jet centre, CV: counter-rotating vortex, RV: rotating vortex, U_r: ejection velocity, U_θ: rotating velocity.

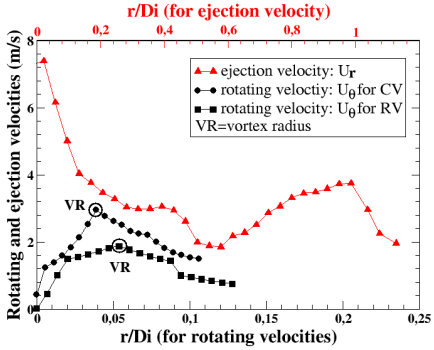

Fig.6: Instantaneous ejection velocity U_r-profile and rotating velocity U_θ-profiles for the couple of streamwise vortices CV and RV detected in the transverse PIV field shown in figure 5.